ARTICLE

Effect of Parent Internal Excitation on Product State Distribution in Methyl Radical Photodissociation at 212.5 nm

Guo-rong Wu[a], Jing-hui Zhang[b], Steven A. Harich[a], Xue-ming Yang[a]*

a. State Key Laboratory of Molecular Reaction Dynamics, Dalian Institute of Chemical Physics, Chinese Academy of Sciences, Dalian 116023; b. Institute of Atomic and Molecular Sciences, Academia Sinica, Taipei 23-166

(Dated: Received on March 8, 2005; Accepted on June 30, 2005)

Photodissociation dynamics of the CH_3 radical at 212.5 nm excitation has been studied experimentally using the H atom Rydberg tagging time-of-flight method. CH_3 radicals are produded by photodissociation of CH_3I at 266 nm. Translational energy distribution and angular distribution for the CH_2 product from CH_3 photodissociation at different vibrational levels via the 3s Rydberg state have been measured. From these distributions, product J state distributions are obtained for photodissociation of different vibrationally excited CH_3 radicals. The effect of parent vibrational as well as rotational excitation on the dissociation dynamics of CH_3 is also investigated in detail. Experimental results in this work show that parent vibrational excitation in the umbrella mode has a significant effect on both rotational excitation and angular distribution of the CH_2 product, while parent rotational excitation has obvious effect only on the angular distribution of CH_2 product.

Key words: High Rydberg state, CH_3 radical, Photodissociation

I. INTRODUCTION

Radical photodissociation is important in many research areas, such as atmospheric chemistry, combustion processes and interstellar chemistry. Experimental investigation of radical photodissociation dynamics is limited by the availability of radical beam sources. Up to now, most of the radical photodissociation experiments using molecular beams are preformed using nozzle tip photolysis or discharge methods, in which the radicals are made during the early stage of the expansion so that radicals can be cooled down during the expansion. The main disadvantage of these methods is that the precursors for the radicals are also in the beam with the radicals, which makes the study of radical photochemistry very difficult when the precursors interfere with radicals. It is, therefore, useful to develop pure radical sources for the study of the radical photochemistry. Pure radical sources for photodissociation dynamics studies can be generated using the negative ion photodetatchment technique developed by Neumark *et al.* [1,2].

The ultraviolet spectroscopy of the methyl radical was first investigated by Herzberg and Shoosmith [3,4]. The strong transition observed at 216 nm was assigned to the 0_0^0 band of the electronic transition from the unpaired $2p_z$ electron to a 3s Rydberg orbital. A flash photolysis absorption study of CH_3 and CD_3 by Callear and Metcalfe provided a more complete assignment of the vibronic bands in $2p_z \rightarrow 3s$ electronic transition [5],even though the broad band at 208 nm in the CH_3 spectrum was not assigned clearly. This electronic transition has also been studied using the multiphoton ionization method by Welge *et al.* [6] and Lin *et al.* [7]. Recently, Westre *et al.* [8] and Settersten *et al.* [9] studied the predissociation dynamics of (0000) level of 3s state of CH_3 radical, the predissociation lifetime of the (0000) level is determined to be around 60 fs, indicating that the predissociation of the excited 3s state is extremely fast.

Orbital correlations in the dissociation of the methyl radical were first examined by Yu *et al.* [10], and it was found that the 3s Rydberg state ($\tilde{B}^2A_1'$) is specifically correlated to the singlet methylene, $CH_2(\tilde{a}^1A_1)$ with a small barrier (about 37.62 kJ/mol) and the ground state methyl radical is correlated to two asymptotic dissociation channels, $CH_2(X^3B_1)+H(^2S)$ and $CH(X^2\Pi)+H_2(^1\Sigma_g^+)$. It is therefore interesting to know whether ground state dissociation plays any significant role in the 3s Rydberg state photodissociation. Photodissociation dynamics of the methyl radical at 193 nm has also been investigated by Lee *et al.* [11] in a molecular beam using photofragment translational spectroscopy. The product translational energy distribution indicated that only singlet CH_2 product, $CH_2(\tilde{a}^1A_1)$, is present. The β parameter of the H atom product angular distribution is determined to be –0.9±0.1, which is indicative of a direct and fast dissociation via the electronic transition from the unpaired $2p_z$ electron to a 3s Rydberg orbital. This is in good agreement with the previous theoretical result [10].

*Author to whom correspondence should be addressed. E-mail: xmyang@dicp.ac.cn

We have recently studied photodissociation of CH_3 [12] using a pure radical source generated by molecular beam CH_3I photodissociation, and reported preliminary results. In this work, we would like to report a more complete experimental study and a more detailed analysis of the CH_3 photodissociation processes using the same experimental method described in Ref.[12].

II. EXPERIMENTAL

The experimental setup has been described in a previous publication [12]. Briefly, a pure CH_3 radical source was produced by photolyzing the CH_3I molecules in the beam using a 266 nm laser source produced by the 4^{th} harmonic YAG output. The advantage of this method is that the CH_3 beam can be very pure in the detection region with very few precursors present. It is necessary to point out that the CH_3 radical generated with this method is a nascent photodissociation product from CH_3I. Therefore, it is not cooled as in the nozzle tip photolysis or discharge methods. This actually allows us to study the photodissociation dynamics of both cold and hot methyl radicals. CH_3I photodissociation has been studied previously extensively and most of the present knowledge on the CH_3I photodissociation dynamics involving the A-band have been provided in several recent theoretical studies [13,14] and a recent review article by Kinsey *et al.* [15]. Very recently, the nascent quantum state product distributions corresponding to both $I(^2P_{3/2})$ and $I^*(^2P_{1/2})$ products have been fully determined by Eppink and Parker using the velocity map imaging technique [16]. There are two groups of CH_3 radicals (fast and slow) corresponding to two I atom product states. In this experiment, both groups of CH_3 radicals were studied. By adjusting the time delay between the CH_3I photolysis laser and the CH_3 photolysis laser, CH_3 radicals with different internal excitation can experimentally be studied. Photodissociation of the CH_3 radical was studied at 212.5 nm using the H atom Rydberg "tagging" Time-of-Flight technique, which was developed in the early 1990s by Welge and co-workers [17]. Detailed descriptions of this technique as used for studying molecular photodissociation can be found in Ref.[18].

The CH_3 photolysis light source was the 212.5 nm laser light that was also used to generate the 121.6 nm light. The CH_3 flight distance before it was photolyzed by the 212.5 nm was about 25 mm. The excitation of the ground state H atom product (n=1) from CH_3 photolysis was made by a two-step excitation scheme to n=45 in this experiment. The 121.6 nm VUV light used in the first step excitation was generated using a two photon resonant four wave mixing scheme in a Kr gas cell, while the second step excitation was made by a 365 nm light source. Very small laser powers for both the 365 and 845 nm light sources were used during the experiment in order to reduce the multiple photon effect in the CH_3 photodissociation process. The neutral Rydberg tagged H atom products from CH_3 photodissociation then flew about 78 cm to reach a Z-stack MCP detector. Angular distribution measurements for the H atom products were made by varying the polarization direction of the 212.5 nm photolysis light using a rotatable half-wave plate. The molecular beam of CH_3I was generated by expanding a 10% mixture of CH_3I and Ar at a stagnation pressure of about 100 kPa through a 0.5 mm diameter pulsed nozzle. The MCP detector in this experiment was fixed in the direction along the CH_3 beam.

III. RESULTS

A. Total H atom product signal *vs.* time delay

Using the experimental method described above, we have measured the total H atom signals from the CH_3 photodissociation at many time delays between the 266 nm CH_3I photolysis laser and the 212.5 nm CH_3 photolysis laser. Figure 1 shows the plot of the total H atom signals versus the time delay between the two photolysis lasers, while Figure 2 shows CH_3 radical translational
energy distribution converted from Fig.1. The total H

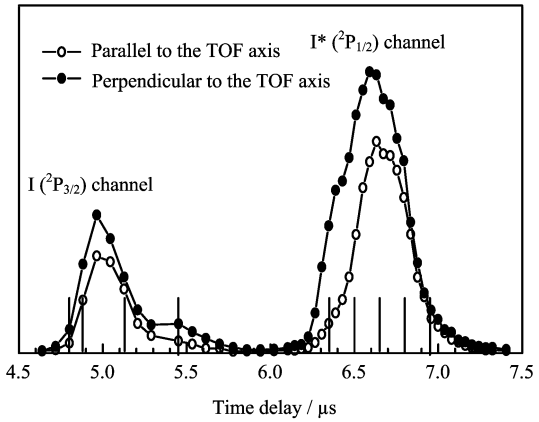

FIG. 1 The delay (between the photolysis laser of CH_3I and the photolysis laser of CH_3) dependence of the total H atom signal from photodissociation of CH_3 radical. The sticks indicate the delays where photodissociation experiment was performed.

atom signal from CH_3 photodissociation is roughly proportional to the density of the CH_3 radical in the dissociation volume. Therefore, Figure 1 is actually the CH_3 time-of-flight spectrum from CH_3I photodissociation at 266 nm, which has been studied previously using other methods. By comparing Fig.2 with the results by Eppink and Parker [16], it is clear that two peaks in Fig.2 are due to the CH_3 radicals generated in the two iodine atom channels, the ground state $I(^2P_{3/2})$ and the first excited state $I^*(^2P_{1/2})$. From earlier CH_3I photodissociation studies at 266 nm, the rovibrational excitation of the CH_3 radical products for both the ground state iodine atoms I and the excited state iodine atoms I^* channels has been determined. Loo and coworkers measured CH_3 (v=0) products rotational temperature for photodissociation of methyl iodine at 266 nm using

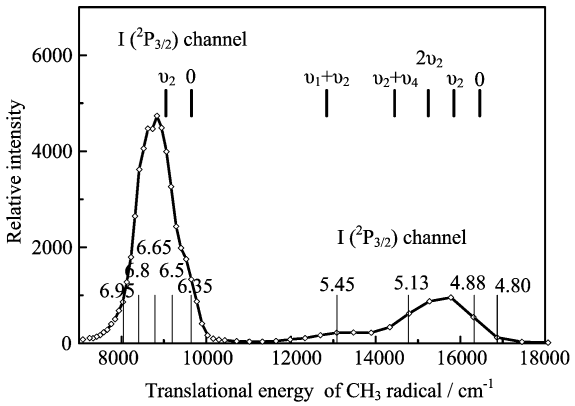

FIG. 2 Product kinetic energy distribution for the CH_3I photodissociation at 266 nm. The lower sticks indicate the energetic limits for different delays(μs) where photodissociation experiment was carried out. The upper sticks indicate the energetic limits for different vibrationally excited CH_3 radical from the photodissociation of CH_3I.

MPI method [19]. The rotational distribution of the total CH_3 products of both two dissociation channels was fitted and a rotational temperature of 120±30 K was extracted. The vibrational state distributions of the CH_3 radical for both dissociation channels have been also measured by various methods. A more recent experimental result was given by Eppink and Parker using velocity map imaging technique. For the I^* channel, vibrational excitation is mainly in the umbrella mode (υ_2), the relative yields of different umbrella vibrational states are υ_2=0:1:2:3=0.63:0.28:0.065:0.02, indicating that more than 90% of CH_3 radicals produced are in the υ_2=0 and υ_2=1 states. As for the I channel, more extensive vibrational excitation for the CH_3 radical was observed. The main vibrational excitation is in the umbrella mode too, and the relative yields of different umbrella vibrational states are υ_2=0:1:2=0.19:0.29:0.22. A slight population inversion in the umbrella mode is indicated. At the same time, excitation of the vibrational mode υ_1 and υ_4 were also observed [16], although the υ_4 mode was not definitely assigned. In the experiment here, the exact vibrational state distribution of the CH_3 product from the two iodine channels could not be determined because of the overlap of the different vibrational excited products. However, some separation of different vibrationally excited CH_3 products is possible. In Fig.2, the translational energy limits for different vibrationally excited CH_3 radicals without rotational excitation are shown. In order to investigate the dissociation dynamics of different vibrationally excited CH_3 radicals, TOF spectra of H atom product were measured carefully at the delay times of 4.80, 4.88, 5.13 and 5.45 μs for the fast group CH_3 (the ground state I($^2P_{3/2}$) atom channel) and 6.35, 6.50, 6.65, 6.80 and 6.95 μs for the slower group CH_3 (excited state I^*($^2P_{1/2}$) atom channel). All signals in the TOF spectra would disappear if the 266 nm CH_3I photolysis laser is blocked, indicating that the signals are all associated with the CH_3 radical photodissociation. Two TOF spectra at each delay were recorded with the CH_3 photolysis laser polarization parallel and perpendicular to the detection axis in order to obtain information on the product anisotropy. The TOF spectrum at the magic angle was also measured in order to obtain the total product translational energy distributions and check the accuracy of the measurement at two polarization directions.

B. Photodissociation of CH_3 radicals from the $I^*(^2P_{1/2})$ channel

In our previous paper,we have concluded from qualitative analyses that the photodissociation dynamics of CH_3 radicals corresponding to the $I^*(^2P_{1/2})$ channel at the two earliest delays 6.35 and 6.50 μs are similar and the CH_3 radicals at these two time delays are mainly at (0000) ground vibrational state, while dynamics at the two latest delays of 6.80 and 6.95 μs are also similar and the CH_3 radicals at these two time delays should be mostly at the (0100) vibrational state with one quantum in the umbrella mode [12]. As for the delay of 6.65 μs, CH_3 radicals are at both the (0000) and (0100) levels. From the energetic limit, we concluded that the CH_2 product from CH_3 photodissociation should be in the $\tilde{a}^1A_1$ state. This conclusion is also consistent with the theoretical picture in which the $CH_3(\tilde{B}^2A_1')$ is correlated to the $CH_2(\tilde{a}^1A_1)$ state [10].

In order to obtain the product rovibrational quantum state information, we have written an interactive simulation program to simulate the product ($CH_2(\tilde{a}^1A_1)$) quantum state distributions. By simulating the two product translational energy distributions shown in Fig.3 at the delays 6.35 and 6.80 μs using the above program, information for product quantum state distributions is extracted. From previous experiments, for CH_3 radicals generated corresponding to the I^* channel, 91% of the CH_3 radicals are in the υ_2=0, 1 levels, with small amount (8.5%) in the υ_2=2, 3 states. Based on estimations from this picture and the simulations, CH_3 radicals arriving at the delay of 6.35 μs should be mainly in the ground vibrational state (0000), while most of the CH_3 radicals arrived at the 6.80 μs delay are mostly in the first excited umbrella mode vibrational state (0100). Figure 3 also shows the simulated product translational energy distributions at the time delays of 6.35 and 6.80 μs using the simulation program. Figure 4 shows the simulated total rotational quantum (J) state distribution of the CH_2 product from the CH_3 photodissociation at these two time delays. The product J state distribution shown here is the summation of the populations in all different k_ak_c states with the same J quantum number for this asymmetric top molecule. In the simulation, all energetically allowed rotational states (different k_ak_c states) of CH_2 product are included. It is clear that if the k quantum numbers are somewhat limited, it would be hard to properly simulate the experimental product translational energy dis-

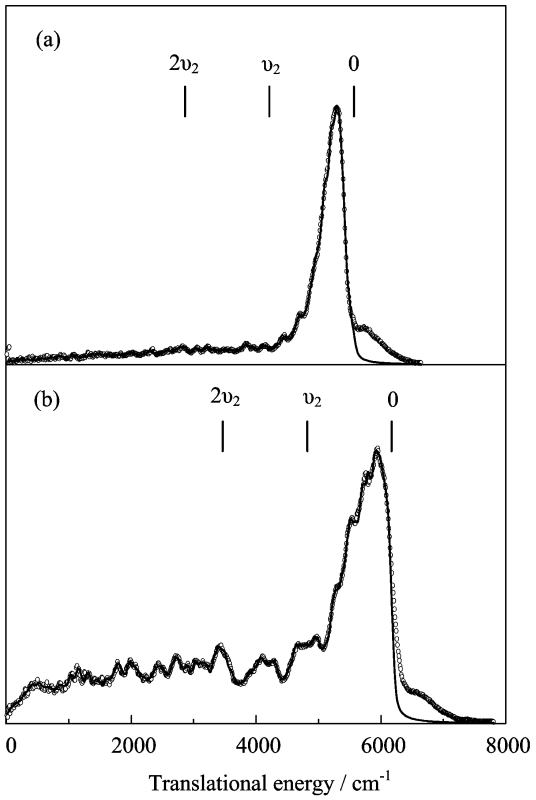

FIG. 3 Experimental (open circles) and simulated (solid line) product translational energy distributions of CH_3 photodissociation at time delays of 6.35 and 6.80 μs. The vertical sticks in (a) and (b) represent the energetic limits for vibrationally excited CH_2 product from the photodissociation of $CH_3(0000)$ and $CH_3(0100)$ respectively.

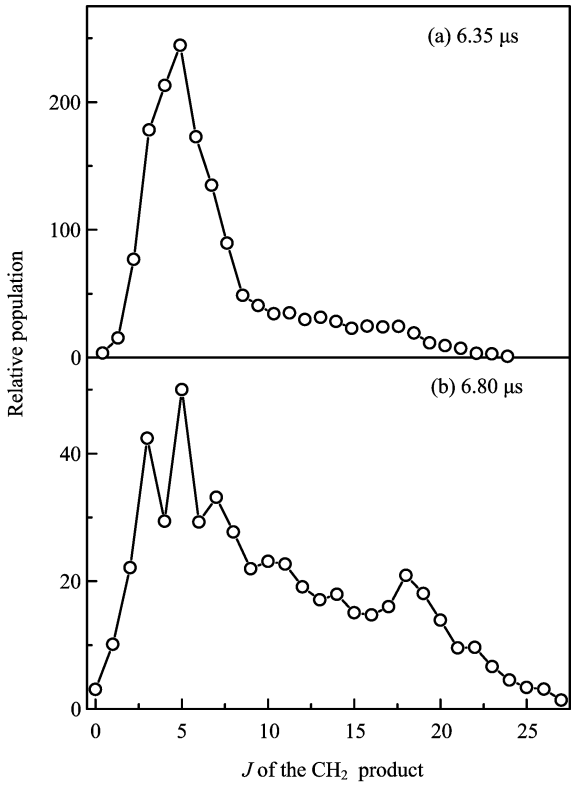

FIG. 4 Simulated product ($CH_2(\tilde{a}^1A_1)$) rotational J quantum state distribution from photodissociation of CH_3 at the (0000) level (a) and the (0100) level (b).

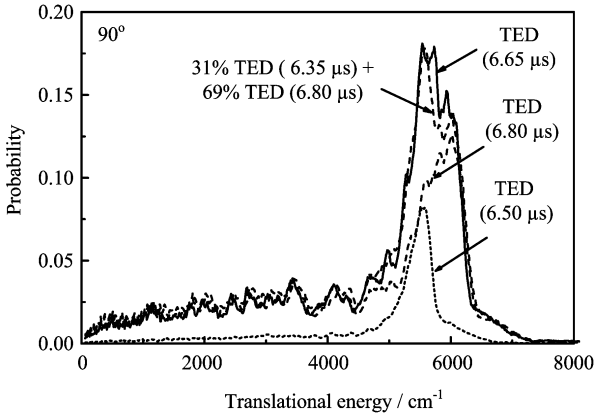

FIG. 5 Product translational energy distribution(TED) at 6.65 μs is compared with a linear combination of that at time delays of 6.50 and 6.80 μs, with a ratio of 31%TED(6.50 μs)+69%TED(6.80 μs).

tribution. Therefore, no evidence for specific k_ak_c state production in the dissociation of CH_3 is observed in this experiment. Because the product translational energy distributions were not well resolved, the derived rotational state distributions bear some uncertainties. However, the general feature of the derived rotational state distributions should be quite reliable. In the experimental translational energy distribution at the delay of 6.35 μs shown in Fig.3 (a), no obvious vibrational structure of the CH_2 product is observed although a few quantum vibrational excitation is energetically allowed. The structures in the translational energy distribution at the delay of 6.80 μs also do not correspond to any product vibrational level clearly (see Fig.3 (b)). Therefore, no vibrationally excited CH_2 products are included in the simulation of the experimental translational energy distributions. This shows that vibrational excitation of the CH_2 product is obviously insignificant. In the simulation, the effect of parent (CH_3) rotational excitation on the product rotational distribution is also neglected because of the similarity of the product translational energy distributions at delays of 6.35 and 6.50 μs and the low rotational temperature of CH_3 raticals. These approximations certainly bring some errors into the rotational state distribution extracted. However, it should not be significant. The product translational energy distribution at 6.65 μs delay (Fig.5) could be simulated using a linear combination of that at 6.50 and 6.80 μs delays with a certain mixed ratio, suggesting that methyl radical at the time delay of 6.65 μs is indeed a mixture of that at the (0000) (6.50 μs) and (0100) levels (6.80 μs). This quantitative analysis strongly supports our conclusions based on qualitative analysis [12].

C. Photodissociation of CH_3 radicals from the $I(^2P_{3/2})$ channel

For photodissociation of CH_3 radicals from the $I(^2P_{3/2})$ channel, TOF spectra were measured carefully at four different delays: 4.80, 4.88, 5.13 and 5.45 μs. The product translational energy distribution at 4.80 μs is very similar to that at the 6.35 μs, as shown in Fig.6, indicating the fastest CH_3 radicals corresponding to the I channel are also in the ground vibrational state. At 4.88 μs delay, the translational energy distribution (Fig.7) is somewhat similar to that at the 6.65 μs, indicating that the CH_3 radicals arriving at this delay is also likely a mixture of the (0000) and (0100) levels. There are also some differences between these two time delays. This is likely due to the difference of the combination ratios of the (0000) and (0100) levels as well as the different rotational excitations at these two time delays.

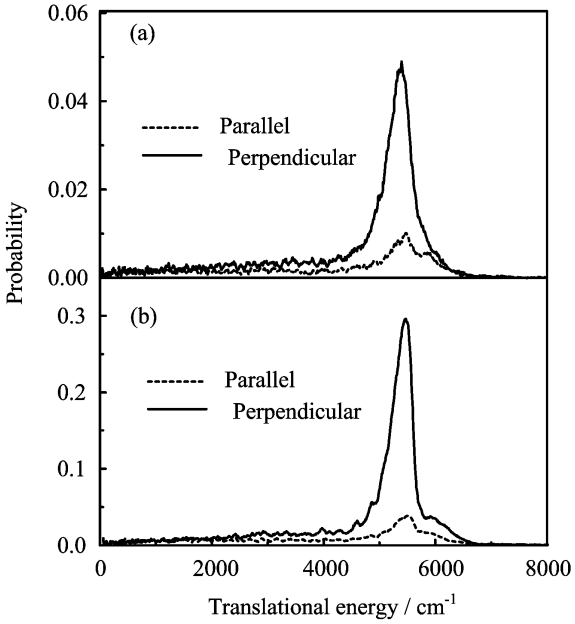

FIG. 6 Comparisons of product translational energy distributions for the CH_3 photodissociation at 212.5 nm at the time delays of 6.35 μs(a) and 4.80 μs(b). The vertical sticks indicate the energetic limits for photodissociation of different vibrationally excited CH_3 ratical.

At the delays of 5.13 and 5.45 μs, the product translational energy distributions at two different polarization directions are shown in Fig.8 and the total product translational energy distributions are shown in Fig.9. The results at these two delays are quite different from other delays (6.50 and 6.80 μs). Qualitatively, this is not difficult to understand. In the $I(^2P_{3/2})$ channel, the umbrella mode of CH_3 is quite excited with populations at three vibrational levels of υ_2=0:1:2=0.19:0.29:0.22. At the 5.13 μs, it is already after the energetic limit of the $2\upsilon_2$ state. Therefore CH_3 arriving at this time delay is probably a mixture of vibrational states of (0100) and (0200) and most of them at (0200) level. The higher

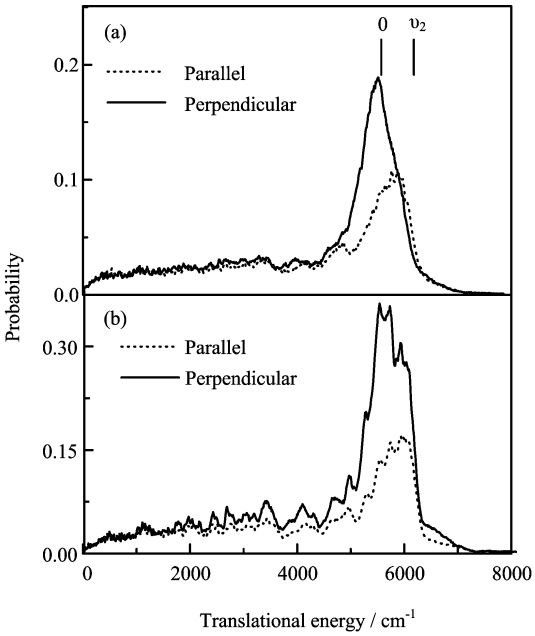

FIG. 7 Comparisons of product translational energy distributions for the CH_3 photodissociation at 212.5 nm at the time delays of 6.35 μs(a) and 4.80 μs(b). The vertical sticks indicate the energetic limits for photodissociation of different vibrationally excited CH_3 radical.

energetic limit of the product translational energy distribution is also consistent with the vibrationally excited $CH_3(0200)$ dissociation. By using a reasonable rotational J state distribution assuming that the CH_3 radical precursors are in the (0100) and (0200) levels, the product translational energy distributions at the delay 5.13 μs can be properly simulated. Figure 9 (a) also shows the simulated product translational energy distributions at this time delay, in comparison with the experimental distribution. At the time delay of 5.45 μs, the CH_3 products correspond to a hump in Fig.2 that can be assigned mainly to the $CH_3(0101)$ and $CH_3(1100)$ products with some small contributions possibly from the (0100) and (0200) levels. There are three obvious peaks in the translational energy distribution at this time delay (see Fig.8 (b) and Fig.9 (b)). The highest energetic limit of the product translational energy distribution is consistent with the vibrationally excited $CH_3(1100)$ dissociation. Therefore, the highest energy peak should come from $CH_3(1100)$ photodissociation. The middle peak is consistent with the energetics of the photodissociation of $CH_3(0101)$. The lowest energy peak is consistent with photodissociation of CH_3 at the (0100) and (0200) levels. By using a reasonable rotational J state distribution and assuming that the CH_3 radical precursor at this time delay is a mixture sample in four vibrational levels: (0101), (1100), (0100) and (0200), the translational energy distribution can be properly simulated (see Fig.9 (b)). Since there are so many product rotational states involved in the translation energy distribution, the product rotational J state

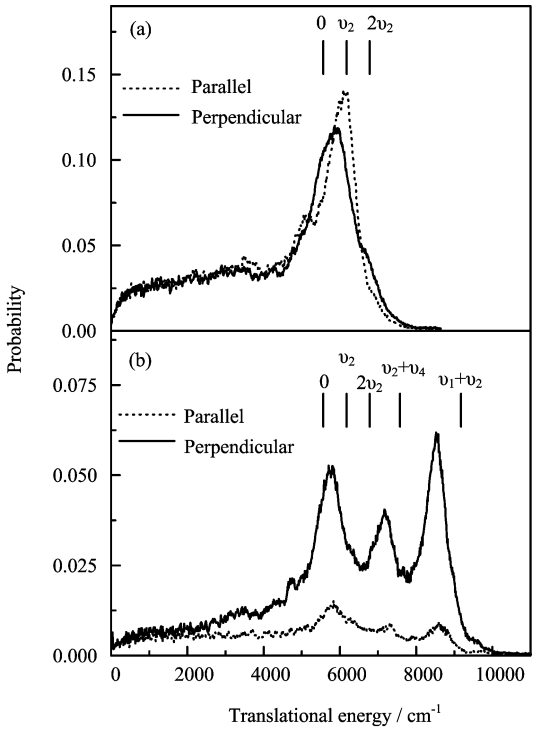

FIG. 8 Experimental product translational energy distributions at two different polarizations for the CH_3 photodissociation at 212.5 nm at the time delays of 5.13 μs(a) and 5.45 μs(b). The vertical sticks indicate the energetic limits for photodissociation of different vibrationally excited CH_3 radical.

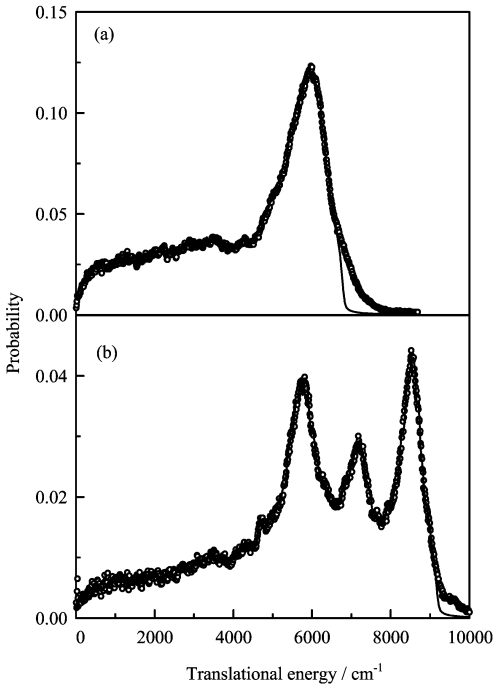

FIG. 9 Experimental (open circles) and simulated (solid line) total product translational energy distributions from photodissociation of CH_3 at the 5.13 μs(a) and 5.45 μs(b).

distributions obtained from this simulation are heavily correlated. Therefore, it is not appropriate to discuss the significance of these distributions. Nevertheless, the simulation does provide a support to the picture we presented above.

D. Energy dependent product angular anisotropy

In addition to the product translational energy distribution, angular distribution also provides important information for photodissociation dynamics. From translational energy distributions measured at two laser polarizations (parallel and perpendicular to the detection direction), the anisotropy parameter can be derived. In this experiment, CH_3 radical came from the photolysis of CH_3I at 266 nm. The orientation of CH_3 radical in dissociation of CH_3I should have no essential effect on the angular distribution of the dissociation products. Since the CH_3 radical had flown for a few μs before it was dissociated, and during the flight period, the CH_3 radical should have rotated many times already. In Fig.10 (a), the dependence of the anisotropy parameter on the translational energy is shown for two time delays: 6.35 and 6.80 μs. One is for photodissociation of $CH_3(0000)$, and the other is for photodissociation of $CH_3(0100)$. Obviously, anisotropy parameters for both cases are translational energy dependent. Overall, the anisotropy parameter for both cases decreases as translational energy increases. The rotationally excited products (low translational energy region) are generated with lower angular anisotropy parameters. There is also the general decrease of the anisotropy parameter values with the increase of the time delay for CH_3 corresponding to the I^* channel. This is due to the effect of the vibrational excitation as well as the rotational excitation of the CH_3 radical in the photodissociation. Figure 10 (b) shows the translational energy dependence of the product angular anisotropy parameters from photodissociation of CH_3 radicals corresponding to the I channel. Obviously the translational energy dependence of the product angular anisotropy at difference time delays is much more complicated. This is likely due to the more complicated nature of the vibrationally excited CH_3 precursors from the I channel than that from the I^* channel. From this result, one can see that the product angular anisotropy in CH_3 photodissociation is heavily dependent on the vibrational characteristics of the CH_3 precursors.

IV. DISCUSSION

A. $CH_2(\tilde{a}^1A_1)$ product vibrational and rotational excitations

From the experimental investigations, extensive rotational excitation are observed without significant vibrational excitation. It is quite clear that most of the available energy in the CH_3 radical is deposited into

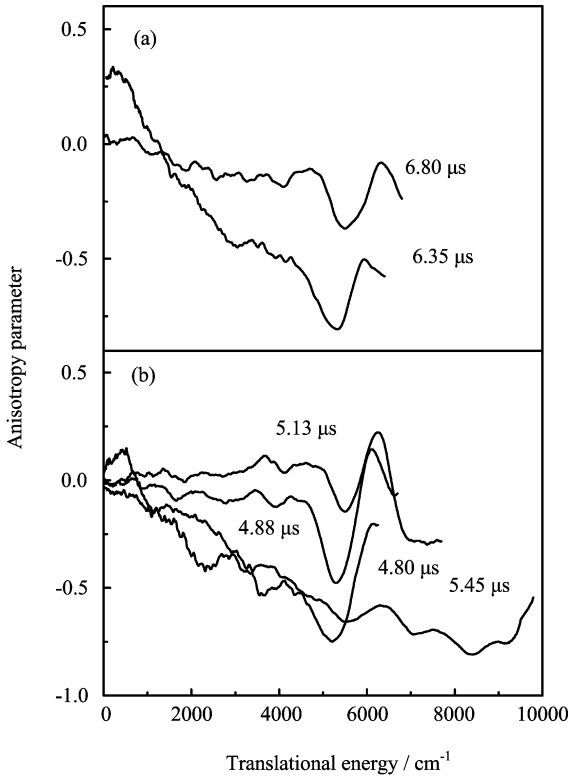

FIG. 10 Energy dependent product angular anisotropy parameter for photodissociation of CH_3 radicals at the time delays of 6.35 and 6.80 μs (a) and 4.80, 4.88, 5.13 and 5.45 μs (b).

the translational degrees of freedom. This is consistent with the theoretical picture of a fast dissociation on a repulsive B state potential energy surface along the C–H dissociation coordinate [10]. Another interesting observation is that the CH_2 product is somewhat rotationally excited with almost no vibrational excitation. From the geometry parameters shown in Table I, the CH bond distances for $CH_3(\tilde{B}^2A_1')$ and $CH_2(\tilde{a}^1A_1)$ are similar, implying that CH stretching vibration is unlikely to be excited in the photodissociation process. It is, however, less obvious that the CH_2 bending vibration is not excited since the H–C–H bond angle for $CH_3(\tilde{B}^2A_1')$ is significantly different from that of $CH_2(\tilde{a}^1A_1)$. One possible reason is that the H–C–H bond angle is changed significantly toward the value of $CH_2(\tilde{a}^1A_1)$ before dissociation, suggesting that the transition state is closer to the product.

TABLE I Geometry parameters of CH_3 and CH_2 radicals

	$CH_3(\tilde{X}^2A_2'')$	$CH_3(\tilde{B}^2A_1')$	$CH_2(\tilde{a}^1A_1)$
$C\cdots H_{1,2}$/Å	1.069	1.082	1.099
$C\cdots H_3$/Å	1.069	1.082	–
$\angle H_1CH_2$/(°)	120	120	105.7

B. Effect of Parent Rotational Excitation

Since the translational resolution is not sufficiently high for the CH_3 precursor selection and the production detection, the effect of parent rotational effect is not easily traceable. However, in one case, this can be traced clearly. Overall, the translational energy distributions at the delays of 6.35 and 6.50 μs are very much similar (Fig.11). As we have pointed above, this is likely due to the fact that CH_3 radicals arriving at these two time delays are all at the ground vibrational level. Therefore the main dynamical feature should be similar for the two time delays. From Fig.2, however, it is shown that the averaged rotational excitation of the CH_3 radicals arriving at 6.50 μs should be significantly larger than that of the CH_3 radicals arrived at 6.35 μs. From the comparison, we can see that the edge of product translational energy at the 6.50 μs is shifted to higher energy by about 250 cm^{-1}. This is likely due to the parent rotational excitation. The shapes of the distributions at these two time delays are, however, almost exactly the same, indicating that parent rotational excitation does not have a significant effect on the product rotational state distribution.

C. Effect of Parent Umbrella Mode Vibrational Excitation

From Fig.3 and Fig.4 , it is very clear that product rotational J state distribution from photodissociation of CH_3 at the ground vibrational level is noticeably different from that at the (0100) level with one quantum in the umbrella mode. The rotational excitation from the umbrella mode excited CH_3 radical is clearly higher than that from the ground vibrational state CH_3 radical. Rotational excitation could come from the direct conversion of the umbrella vibration into rotation through a C_{2v} pathway or direct dissociation through a non C_{2v} pathway. The umbrella vibration would provide a torque in the dissociation leading to

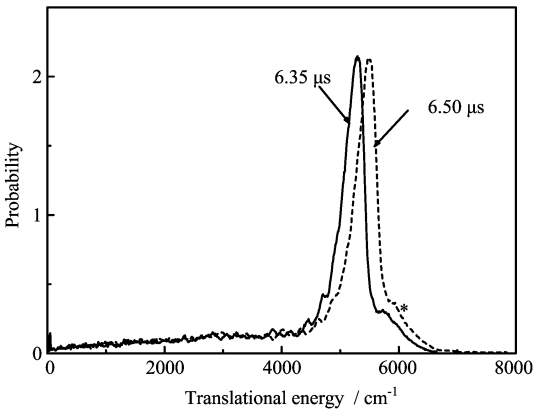

FIG. 11 Comparisons of product total translational energy distributions for the CH_3 photodissociation at 212.5 nm at the time delays of 6.35 and 6.50 μs .

fragment rotation about an axis perpendicular to the C_3 axis. Clearly, the more vibrational excitation in umbrella mode the CH_3 radical is, the more rotational excitation the CH_2 product is. In the photodissociation of other vibrational mode excited radicals, we have no clear experimental evidence that vibrational excitation will enhance product rotational excitation.

V. CONCLUSIONS

Photodissociation dynamics of the CH_3 radical at 212.5 nm excitation was investigated using the H atom Rydberg tagging time-of-flight method with a pure CH_3 radical source from the CH_3I photodissociation at 266 nm. Product translational energy distribution and angular anisotropy distribution for the CH_2 product from CH_3 photodissociation at different vibrational levels via the 3s Rydberg state have been determined from the TOF spectra of the H atom product. From these distributions, product J state distributions are obtained for decomposition of different vibrationally excited CH_3 radicals. Parent vibrational excitation in the umbrella mode seems to have a significant effect on the dissociation dynamics, while effect of parent rotational excitation on the dissociation dynamics is limited. Experimental results also indicate that CH_2 product is essentially not vibrationally excited with significant rotational excitation.

VI. ACKNOWLEDGMENT

This work was supported by the Chinese Academy of Sciences, the Ministry of Science and Technology, and the National Natural Science Foundation of China (No.29973044).

[1] D. L. Osborn, H. Choi, and D. M. Neumark, Adv. Chem. Phys. **101**, 729 (1997).
[2] D. L. Osborn, D. H. Mordaunt, H. Choi, R. T. Bise, D. M. Neumark and C. M. Rohlfing, J. Chem. Phys. **106**, 10087 (1997).
[3] G. Herzberg and J. Shoosmith, Can. J. Phys. **34**, 523 (1956).
[4] G. Herzberg, Proc. R. Soc. London, Ser. A **262**, 291 (1961).
[5] A. B. Callear and M. P. Metcalfe, Chem. Phys. **14**, 275 (1976).
[6] J. Danon, H. Zacharias, H. Rottke and H. H. Welge, J. Chem. Phys. **76**, 2399 1982.
[7] T. G. DiGiuseppe, J. W. Hudgens and M. C. Lin, J. Phys. Chem. **86**, 36 1982.
[8] S. G. Westre, P. B. Kelly, Y. P. Zhang and L. D. Ziegler, J. Chem. Phys. **94**, 270 (1991).
[9] T. B. Settersten, R. L. Farrow and J. A. Gray, Chem. Phys. Lett. **170**, 104 (2003).
[10] H. T. Yu, A. Sevin, E. Kassab and E. M. Evleth, J. Chem. Phys. **80**, 2049 (1984).
[11] S. W. North, D. A. Blank, P. M. Chu and Y. T. Lee, J. Chem. Phys. **102**, 792 (1995).
[12] G. R. Wu, B. Jiang, Q. Ran, J. H. Zhang, S. A. Harich and X. M. Yang, J. Chem. Phys. **120**, 2193 2004.
[13] A. D. Hammerich, U. Manthe, R. Kosloff, H. D. Meyer and L. S. Cederbaum, J. Chem. Phys. **101**, 5623 (1994).
[14] Y. Amatatsu, K. Morokuma and S. Yabushita, J. Chem. Phys. **94**, 4858 (1991); Y. Amatatsu, S. Yabushita and K. Morokuma, ibid. **104**, 9783 (1996).
[15] B. R. Johnson, C. Kittrell, P. B. Kelly and J. L. Kinsey, J. Phys. Chem. **100**, 7743 (1996).
[16] A. T. J. Eppink and D. H. Parker, J. Chem. Phys. **110**, 832 (1999).
[17] L. Schnieder, W. Meier, K. H. Welge, M. N. R. Ashfold and C. M. Western, J. Chem. Phys. **92**, 7027 (1990).
[18] M. N. R. Ashfold, D. H. Mordaunt and S. H. S. Wilson, *Advances in Photochemistry*, edited by D. C. Neckers, D. H. Volman and G. V. Bunau, New York: Wiley, **21**, 217 (1996).
[19] L. R. Ogorzalek, H. P. Haerri, G. E. Hall and P. L. Houston, J. Chem. Phys. **90**, 4222 (1989).